Asociación Argentina
de Mecánica Computacional

Mecánica Computacional Vol XXIX, págs. 8429-8445 (artículo completo)
Eduardo Dvorkin, Marcela Goldschmit, Mario Storti (Eds.)
Buenos Aires, Argentina, 15-18 Noviembre 2010

ASYMPTOTIC APPROACH FOR MODELLING PROGRESSIVE CAVITY PUMPS PERFORMANCE

Selma F. Andrade[a], Juliana V. Valério[b] and Márcio S. Carvalho[c]

[a]*E e P - Petrobrás, selmafaa@petrobras.com.br, http://www.petrobras.com.br*

[b]*Departamento de Ciência da Computação,Instituto de Matemática, UFRJ, PO Box:68.530, RJ-21941-590 - Brasil, juvianna@dcc.ufrj.br, http://www.dcc.ufrj.br*

[c]*Departamento de Engenharia Mecânica, PUC-Rio, R. Mq. S. Vicente 225, Rio de Janeiro, 22453-900, Brasil, msc@puc-rio.br, http://www.mec.puc-rio.br*

Keywords: Progressive cavity pumps, Lubrication theory, Asymptotic model

Abstract. The fundamental understanding of the flow inside Progressive Cavities Pumps (PCP) represents an important step on the optimization of the efficiency of these pumps, which are largely used in artificial lift processes in the petroleum industry. The computation of the flow inside a PCP is extremely complex due to the transient character of the flow, the moving boundaries and the difference in length scale of the channel height between the stator and rotor. This complexity makes the use of computational fluid dynamics as an engineering tool almost impossible. This work presents an asymptotic model to describe the single phase flow inside progressive cavities pumps using lubrication theory. The model was developed for Newtonian fluid and lubrication theory was used to reduce the three-dimensional Navier-Stokes equations in cylindrical coordinates to a two-dimensional Poisson's equation for the pressure field at each time step, which is solved numerically by a second order finite difference method. The predictions are close to the experimental data and the results obtained by solving the complete three-dimensional, transient Navier-Stokes equations with moving boundaries, available in the literature. Although the accuracy is similar to the complete 3D model, the computing time of the presented model is orders of magnitude smaller. The model was used to study the effect of geometry, fluid properties and operating parameters in the pump performance curves and can be used in the design of new pumping processes.

1 INTRODUCTION

Almost every fluid-like material can be pumped with Progressive Cavity Pumps (PCP). Since the pumping principle conceived by the René Moineau in the 1930‘s, a large number of different industrial applications makes this positive displacement pump on of the most used technologies for moving fluids, from sandy crude oil to waste sludge. PCPs in their simplest form consist of a single threaded screw (rotor), turning inside a double threaded nut (stator), forming consecutive cavities separated by seal lines, as illustrate in figure 1. This simple configuration belongs to the singlelobe category of PCP. More complex geometries with a larger number of lobes are also used, and any combination is possible as long as the stator has one more lead than the rotor. The first generation of PCPs had a metallic rotor and stator, forming rigid moving cavities in the space between the two surfaces. The following generations presented a rubber covered stator, which is common nowadays. The deformable stator creates a compression fit with the rotor, in contrast with the metallic pump where there is a small clearance leading to a larger leakage between consecutive cavities. Considering that deformable stators have operational limitations related with temperature and mechanical resistance of the elastomers, metallic PCPs have been recognized by the oil industry as an important technological alternative for heavy oil production. This apparently simple mechanism produces an almost pulsation-free positive displacement flow, without the need for valves, based on the movement of the cavities from the suction to the discharge ends of the pump as the rotor turns inside the stator. The volumetric flow delivered by a PCP at a constant rotor speed and pressure difference depends on three design features: rotor diameter, rotor eccentricity and stator pitch. The pump pressure rating depends on the number of stages. A peculiar characteristic of PCPs is the occurrence of back flow, also denominated slip flow, derived from non perfectly sealed cavities.

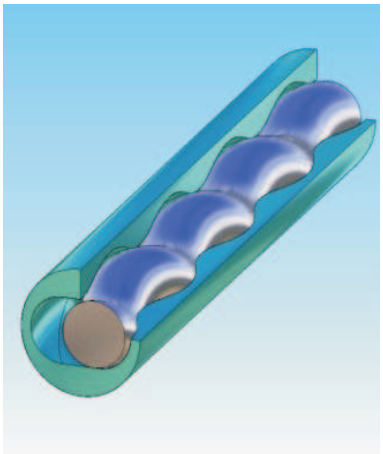

Figure 1: Components of PCP

Due to their unique design and principle of operation, PCPs provide many benefits in oilfield applications, such as high solid content tolerance, best efficiency with high viscosity fluids, simple installation and operation. Oil production with PCPs is generally designed over the knowledge of characteristic pump curves provided by manufacturer, but several variables can affect and change the volumetric efficiency of both metallic and elastomeric stator pumps. It is common knowledge that the characteristic curves change significantly with liquid viscosity and gas content, therefore pump curves provided by manufacturers usually do not represent the

real pump performance at down hole conditions. Moreover, in order to design PCPs that can be operated at extreme conditions, it is important to understand the effect of each geometric design parameter on the pump performance. These are the main reasons behind research efforts dedicated to study the flow inside PCPs.

The performance of PCPs is a function of the volumetric pump displacement and the slip flow, i.e. the backward flow between consecutive cavities due to the adverse pressure gradient along the pump. The limitation of simple models on predicting pump performance is related to the difficulties in calculating the internal back flow. For any type of stator, rigid or deformable, slippage is a function of the fluid characteristics, the differential pressure, the dimensions of the different components and the rotor's kinematics. In the case of elastomeric stators the problem become even more complex, because the geometry of the flow channel becomes a function of the pressure field.

In order to estimate the back flow, Sopilka et al. (2002) performed an experimental study and obtained characteristic curves and instantaneous pressure profiles along a metal PCP for single- and two-phase flow conditions.

The first and simplest numerical model to describe the flow inside a PCP was presented by Moineau, 1930 Moineau and it is based on calculating the back flow across the pump, considering a Hagen-Poiseuille flow through the seal lines, which is subtracted from the volume displaced by the rotating rotor, giving the volumetric flow rate. As the differential pressure across the pump rises, so does the slippage, and the relation between differential pressure and net volumetric flow pumped, can be calculated. Since the slippage gap area is not clearly defined, the model is able to describe the qualitative behavior, but it is not accurate.

The volumetric displacement associated with the rotor movement can be easily calculated from pump component's geometry, but calculating the back flow is not a trivial problem. In order to improve Moineau's model, Blanco and Olivet (2003) have modeled the slip as the superposition of two different mechanism: one due to the rotor's movement and the other due to the differential pressure between two cavities. However, limitations were recognized and the model was not able to fit experimental data.

Only recently, a complete three-dimensional, transient model of the flow inside the cavities of a PCP has been presented Paladino et al. (2008). The numerical solution obtained with a commercial CFD software is extremely complex and computationally expensive, mainly because of the transient and 3-D character of the flow, the complexity of the geometry and the necessary mesh motion to follow the rotor movement. The results agree well with experimental data, however the use of the model for testing different operating conditions and pump designs is limited, since the time to compute the flow at a single operating condition was extremely high. Therefore, the time required to produce an entire pump performance curve would be enormous.

Realizing that the back flow, that ultimately defines the flow rate - pressure drop relationship, is governed by what happens in the small clearance between the moving rotor and the stator and that the ratio of length scale in the flow direction to the channel height in this region is very large, we propose an asymptotic model to describe the flow inside PCPs. The proposed model reduces the three-dimensional transient Navier-Stokes equations with moving boundaries to a quasi-steady state two-dimensional Poisson's equation for the pressure field inside the pump.

This is the same idea behind simplified models of the flow in screw extruder - see Li Y. (1996) and Suresh A. (2008). The simplified models for extruder can predict the qualitative behavior, but they are still not accurate enough to use as a design tool, mainly because of the geometric and kinematic simplifications used. One of the common hypothesis is to neglect the curvature effect of the cross section, and to describe the geometry of the flow region us-

ing cartesian coordinates. Carvalho and de Pina (2006) presented a lubrication approximation model in cylindrical coordinates to describe the flow in annular space with varying eccentricity and showed that neglecting the curvature effect can greatly compromise the accuracy of the model.

The goal of this work is to develop an asymptotic model for the flow inside a metallic (rigid) singlelobe progressive cavity pump. The cross section is parameterized using cylindrical coordinates and there is no simplified assumptions on the geometry and kinematics of the rotor. The resulting 2D equation for the pressure field at each time step was discretized with a second order finite difference approximation. The model was used to obtain predictions of the pump performance curve as a function of rotor speed, liquid properties and pump geometry.

The results obtained agree very well with the experimental data and also with the complete 3D model. However the computational time required was approximately 100 times smaller.

2 MATHEMATICAL MODELLING

The flow inside the pump cavities is governed by the Navier-Stokes and continuity equations, which in cylindrical coordinates are:

$$\frac{1}{r}\frac{\partial rv}{\partial r}+\frac{1}{r}\frac{\partial w}{\partial \theta}+\frac{\partial u}{\partial z}=0,$$

$$\rho\left(\frac{\partial u}{\partial t}+u\frac{\partial u}{\partial z}+v\frac{\partial u}{\partial r}+\frac{w}{r}\frac{\partial u}{\partial \theta}\right)=\rho g_z-\frac{\partial p}{\partial z}+\mu\left\{\frac{1}{r}\frac{\partial}{\partial r}\left(r\frac{\partial u}{\partial r}\right)+\frac{1}{r^2}\frac{\partial^2 u}{\partial \theta^2}+\frac{\partial^2 u}{\partial z^2}\right\},$$

$$\rho\left(\frac{\partial v}{\partial t}+v\frac{\partial v}{\partial r}+u\frac{\partial v}{\partial z}+\frac{w}{r}\frac{\partial v}{\partial \theta}-\frac{w^2}{r}\right)=\rho g_r-\frac{\partial p}{\partial r}+\quad\mu\left\{\frac{\partial}{\partial r}\left(\frac{1}{r}\frac{\partial}{\partial r}(rv)\right)+\frac{1}{r^2}\frac{\partial^2 v}{\partial \theta^2}-\frac{2}{r^2}\frac{\partial w}{\partial \theta}+\frac{\partial^2 v}{\partial z^2}\right\},$$

$$\rho\left(\frac{\partial w}{\partial t}+v\frac{\partial w}{\partial r}+u\frac{\partial w}{\partial z}+\frac{w}{r}\frac{\partial w}{\partial \theta}-\frac{vw}{r}\right)=\rho g_\theta-\frac{1}{r}\frac{\partial p}{\partial \theta}+\mu\left\{\frac{\partial}{\partial r}\left(\frac{1}{r}\frac{\partial (rw)}{\partial r}\right)+\frac{1}{r^2}\frac{\partial^2 w}{\partial \theta^2}-\frac{2}{r^2}\frac{\partial v}{\partial \theta}+\frac{\partial^2 w}{\partial z^2}\right\}.$$

where u, v, and w are the axial, radial, and tangential velocity components; p is the liquid pressure and ρ and μ are the liquid density and viscosity. To avoid solving the system of coupled three-dimensional differential equations, dimensional analysis is used to eliminate some of the terms. The procedure used here is generally known as lubrication approximation.

Along the seal lines between consecutive cavities, the clearance between the rotor and stator is much smaller than the radius or length of the pump: $\delta = (R_o - R_r) \ll R_o \sim R_r \leq L$, as shown in figure 2.

Using the continuity equation, it can be shown that the main flow is in the axial direction, the velocity component in the radial direction is much smaller than in the other two, i.e. $u, w \gg v$. Moreover, the variation of the velocity components in the axial and azimuthal directions are much smaller than those in the radial direction. Thus, the derivatives with respect to the radial direction are much larger than the others; $\dfrac{\partial^2 u}{\partial r^2} \gg \dfrac{\partial^2 u}{\partial z^2}, \dfrac{\partial^2 u}{\partial \theta^2}$ and $\dfrac{\partial^2 w}{\partial r^2} \gg \dfrac{\partial^2 w}{\partial z^2}, \dfrac{\partial^2 w}{\partial \theta^2}$.

By applying dimensional analysis, the appropriate terms of the transient Navier-Stokes equations can be neglected and the system of differential equations become:

$$0=-\frac{\partial p}{\partial z}+\mu\left[\frac{1}{r}\frac{\partial}{\partial r}\left(r\frac{\partial u}{\partial r}\right)\right],\ 0=-\frac{\partial p}{\partial r},\ 0=-\frac{1}{r}\frac{\partial p}{\partial \theta}+\mu\left[\frac{\partial}{\partial r}\left(\frac{1}{r}\frac{\partial (rw)}{\partial r}\right)\right]. \qquad (1)$$

Since the pressure is not a function of r, the velocities u and w can be analytically integrated in the radial direction as a function of the pressure gradient:

$$u=\left(\frac{\partial p}{\partial z}-\rho g\right)\frac{1}{4\mu}r^2+c_1\ln r+c_2;\quad w=\frac{1}{2\mu}\frac{\partial p}{\partial \theta}\left(\ln r-\frac{1}{2}\right)+\frac{c_3}{2}r+\frac{c_4}{r}; \qquad (2)$$

where c_1, c_2, c_3, c_4 are constants calculated based on the boundary conditions, which are discussed in the following sub-section.

2.1 Pump Geometry and Integral Limits

The movement of the fluid inside the pump is caused by the single-threaded helical rotor rolling eccentrically inside a helical double-threaded stator. As the stator has a pitch length twice as long as the rotor is, the fluid is trapped in consecutive quasi-sealed cavities. These cavities follow each other and produce an almost pulsation-free, positive displacement flow, as sketched in figure 1.

The flow displacement inside a PCP depends on three design parameters: Rotor radius (R_r), eccentricity (E) and stator pitch (P_{st}), as defined in figure 2. The center of the rotor's helix (center of mass of the rotor) rotates around the center of the stator. The distance between these two points defines the eccentricity (E). It is important to notice that the center of each cross section of the rotor is not its center of mass, as sketched in figure 2.

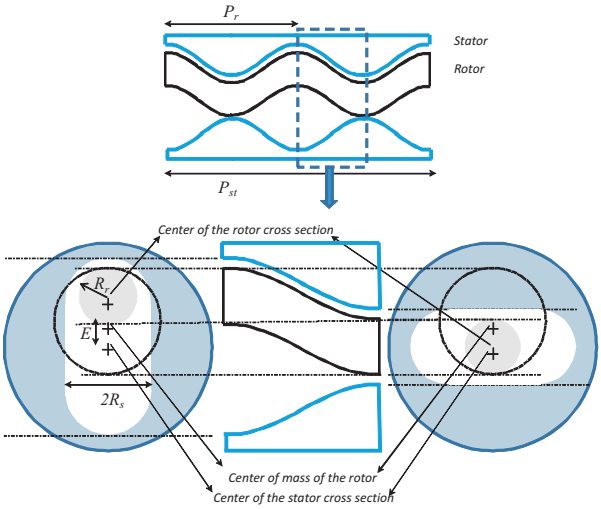

Figure 2: PCP's cross section.

In each cross section, the origin of the coordinate system lies on the center of the cross section of the rotor (C_r), therefore its location and the coordinates of the stator wall with respect to the origin varies with time, as the rotor rotates, as illustrated in the figure 3. The figure shows the movement of the center of the rotor cross section and of a poit P located on the surface of the rotor during one rotation.

Eventhough the velocity component in the radial direction, v, is much smaller compared to the others, in the boundary conditions it needs to be considered in order to describe the relative movement of the rotor with respect to the stator.

The geometry of each cross section of the pump cavity is defined with respect to the cylindrical coordinate system adopted here, through the geometry of the rotor wall $R_r(\theta, z)$ and of the stator wall $R_o(\theta, z)$ as shown in figure 4. Because of the origin of the coordinate system is located at the center of the rotor's cross section $R_r(\theta, z) = R_r$ is constant. The definition of the stator wall geometry $R_o(\theta, z)$ is not simple because of the complex geometry and kinematics of the pump elements.

Some important variables used to describe the position of the surface of the stator, $R_o(\theta, z)$,

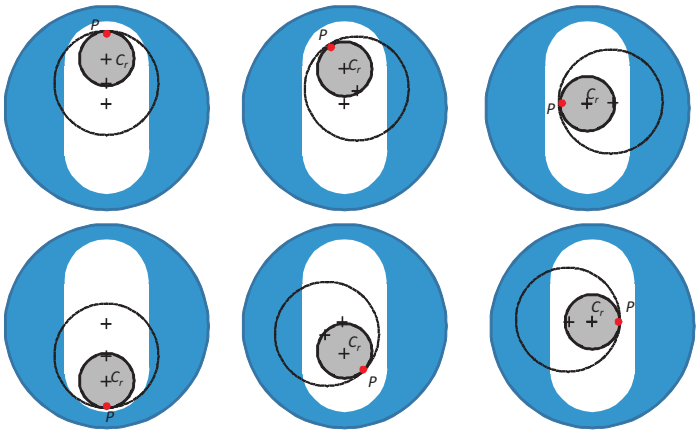

Figure 3: Rotation and translation of the rotor.

are shown in figures 4 and 5 and are defined below:

- $\Theta_S = \dfrac{2\pi z}{P_{st}} = \dfrac{\pi z}{P_r}$ is the angle between an horizontal axis passing through C_r to the symmetry line of the stator cross section; P_{st} and P_r are respectively the stator and rotor piches;
- $d_{CSR} = \overline{C_s C_r} = 2E\cos(\Omega t - \Theta_S)$, so $-2E \leq d_{CSR} \leq 2E$ is the distance between the centers of the rotor and stator cross sections;
- $\alpha_1 = \arctan\left(\dfrac{R_s}{2E - d_{CSR}}\right)$ and $\alpha_2 = \arctan\left(\dfrac{R_s}{2E + d_{CSR}}\right)$ are the angles between the symmetry line and the segments $\overline{C_r A}$ to $\overline{C_r A'}$ and $\overline{C_r B}$ to $\overline{C_r B'}$, respectively (see fig 5).

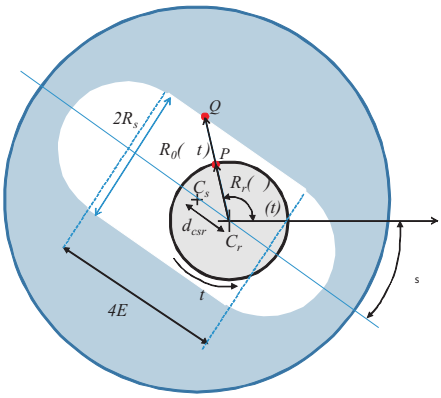

Figure 4: Geometrical elements of the PCP's cross section

In each cross section, the boundary of the stator $R_o(\theta, z)$ is spliced in four parts, as shown in figure 5. Each part is represented by a different function, shown in table 1, which also shows the θ's limits of each segment. In the table, A = $(\alpha 1 - \Theta_s)$; B = $(\pi - \Theta_s - \alpha 2)$; B' = $(\pi + \alpha 2 - \Theta_s)$; A' = $(2\pi - \alpha 1 - \Theta_s)$.

Table 1: The functions that describes the geometry of a singlelobe metal PCP.

Region	θ limits	Function —— $R_o(\theta, z)$
I	A' $\leq \theta <$ A	$(2E - d_{csr})\cos(\theta - \Theta_S) + \sqrt{R_s^2 - (2E - d_{csr})^2 \sin^2(\theta - \Theta_S)}$
II	B $\leq \theta <$ B'	$-(2E + d_{csr})\cos(\theta - \Theta_S) + \sqrt{R_s^2 - (2E + d_{csr})^2 \sin^2(\theta - \Theta_S)}$
III	A $\leq \theta <$ B	$\sqrt{R_s^2 + (2E - d_{csr})^2}\left[\frac{\sin\alpha_1}{\sin(\theta - \Theta_S)}\right]$
IV	B' $\leq \theta <$ A'	$-\sqrt{R_s^2 + (2E - d_{csr})^2}\left[\frac{\sin\alpha_1}{\sin(\theta - \Theta_S)}\right]$

2.2 Rotor Kinematics and Boundary Conditions

As discussed before, the cross section of the rotor translates and rotates with respected to the center of the stator.To derive the appropriate boundary conditions, used to calculate c_1, c_2, c_3 and c_4 in equation (2), we need to determine the velocity of a point P located at the boundary of the rotor and of a point Q at the stator, as shown in figure 5.

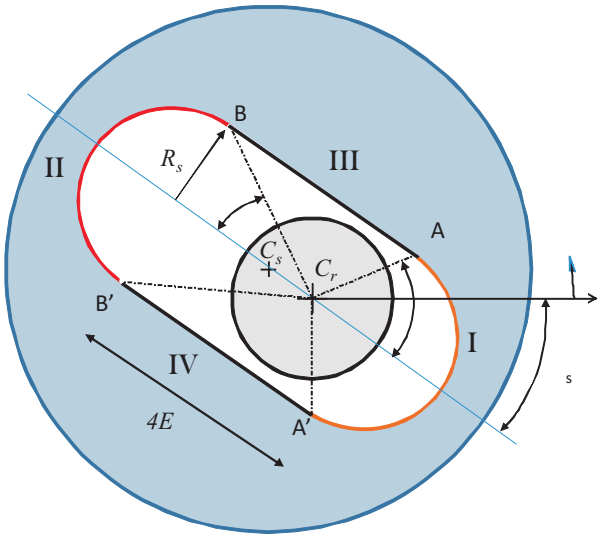

Figure 5: Variables to describe rotor's kinematic

The angular coordinate of P is $\theta(t) = \gamma + \Omega t$, where γ is angular coordinate at $t = 0$ and Ω is the clockwise rotor angular velocity. The cartesian coordinates of the rotor center (our center of reference) with respect to the stator's center (which is stationary in a laboratory frame of reference) is:

$X_{csr} = d_{csr}\cos(\Theta_s) = +2E\cos(\Omega t - \Theta_s)\cos(\Theta_s)$,
$Y_{csr} = -d_{csr}\sin(\Theta_s) = -2E\cos(\Omega t - \Theta_s)\sin(\Theta_s)$.

Thus the velocity of the rotor center is: $\overrightarrow{V_{csr}} = V_{X_{csr}}\,\overrightarrow{i} + V_{Y_{csr}}\,\overrightarrow{j} = (V_{X_{csr}}, V_{Y_{csr}})$:
$V_{X_{csr}} = -2E\Omega\sin(\Omega t - \Theta_s)\cos(\Theta_s)$, $\quad V_{Y_{csr}} = 2E\Omega\sin(\Omega t - \Theta_s)\sin(\Theta_s)$.

So, $(X_P, Y_P) = (X_{csr} + R_r\cos(\gamma + \Omega t), Y_{csr} + R_r\sin(\gamma + \Omega t))$ is the position of the point P related to the stator center and its velocity is $\overrightarrow{V_P} = (V_{X_P}, V_{Y_P})$: $\quad V_{X_P} = V_{X_{csr}} - R_r\Omega\sin\theta$, $\quad V_{Y_P} = V_{Y_{csr}} + R_r\Omega\cos\theta$.

It is clear that the velocity of P with respect to the frame of reference, the rotor center C_r, is: $\overrightarrow{V_{P_{csr}}} = (V_{X_P} - V_{X_{csr}},\ V_{Y_P} - V_{Y_{csr}}) = (-R_r\Omega\sin\theta,\ R_r\Omega\cos\theta)$.

Similarly, the velocity of the point Q (located at the stator boundary), with respect to the coordinate system, is: $\overrightarrow{V_{Qcsr}} = \overrightarrow{V_Q} - \overrightarrow{V_{csr}}$. Note that $\overrightarrow{V_Q} = 0$, because the stator is stationary with respect to a laboratory frame of reference, therefore $\overrightarrow{V_{Qcsr}} = -\overrightarrow{V_{csr}} = (2E\Omega\sin(\Omega t - \Theta_s)\cos(\Theta_s), -2E\Omega\sin(\Omega t - \Theta_s)\sin(\Theta_s))$

In order to write the formulation in cylindrical coordinates, the velocity of points along the rotor (P) and stator (Q) surfaces written in cartesian coordinates are presented in cylindrical coordinates following the transformation matrix below:

$$\begin{bmatrix} V_r \\ V_\theta \end{bmatrix} = \begin{bmatrix} \cos\theta & \sin\theta \\ -\sin\theta & \cos\theta \end{bmatrix} \begin{bmatrix} V_x \\ V_y \end{bmatrix}$$

Therefore the appropriate boundary conditions for equations (2) are:

$$u(R_o) = 0$$

$$v(R_o) = V_{X_{Qcsr}}\cos\theta + V_{Y_{Qcsr}}\sin\theta = +2E\Omega\sin(\Omega t - \Theta_s)\cos(\Theta_s)$$
$$w(R_o) = -V_{X_{Qcsr}}\sin\theta + V_{Y_{Qcsr}}\cos\theta = -2E\Omega\sin(\Omega t - \Theta_s)\sin(\Theta_s)$$

$$\begin{aligned} u(R_r) &= 0 \\ v(R_r) &= V_{X_{Pcsr}}\cos\theta + V_{Y_{Pcsr}}\sin\theta = 0 \\ w(R_r) &= -V_{X_{Pcsr}}\sin\theta + V_{Y_{Pcsr}}\cos\theta = \Omega R_r \end{aligned} \tag{3}$$

As expected, with respect to the center of the rotor cross section, P does not move in the radial direction. Also, points along the stator and rotor surfaces do not move axially.

Back to equations (2) and applying the boundary conditions presented in equations (3), we are able to find c_1, c_2, c_3, c_4 and write the complete expressions for the velocity profiles u and w:

$$u = \left(\rho g - \frac{\partial p}{\partial z}\right)\frac{R_i^2}{4\mu}\left\{1 - \left(\frac{r}{R_i}\right)^2 + \left[\left(\frac{(R_o/R_i^2) - 1}{\ln(R_o/R_i)}\right)\ln\left(\frac{r}{R_i}\right)\right]\right\} \tag{4}$$

$$w = \frac{\partial p}{\partial\theta}\frac{R_r}{2\mu}\left\{\frac{r}{R_r}\left[\ln(r) - \frac{1}{2} + \frac{r}{R_r}K - \frac{R_r}{r}\left(\ln(R_r) - \frac{1}{2} + K\right)\right]\right\} + \left(\frac{W_{Ro}R_o - \Omega R_r^2}{R_o^2 - R_r^2}\right)\left(r - \frac{R_r^2}{r}\right) + \Omega\frac{R_r^2}{r} \tag{5}$$

where K is the geometric parameter defined as

$$K = \frac{-R_o^2\left(\ln R_o - 1/2\right) + R_r^2\left(\ln R_r - 1/2\right)}{R_o^2 - R_r^2}. \tag{6}$$

Up to this point, the pressure field is still unknown. In order to evaluate it, the continuity equation is integrated along the radial direction, from R_r to R_o:

$$\int_{R_r}^{R_o}\left\{\frac{\partial rv}{\partial r}+\frac{\partial w}{\partial \theta}+\frac{\partial ru}{\partial z}\right\}\mathrm{dr}=0\Rightarrow \underbrace{\int_{R_i}^{R_o}\frac{\partial rv}{\partial r}\,\mathrm{dr}}_{\mathrm{I}}+\underbrace{\int_{R_r}^{R_o}\frac{\partial w}{\partial \theta}\,\mathrm{dr}}_{\mathrm{II}}+\underbrace{\int_{R_r}^{R_o}\frac{\partial ru}{\partial z}\,\mathrm{dr}}_{\mathrm{III}}=0 \tag{7}$$

where $\mathrm{I} = R_o v(R_o) - R_r v(R_r)$,

$$\mathrm{II} = \frac{\partial}{\partial\theta}\int_{R_r}^{R_o} w\,\mathrm{dr} - \left[w(R_o)\frac{\partial R_o}{\partial\theta} - w(R_r)\frac{\partial R_r}{\partial\theta}\right]$$

$$\mathrm{III} = \frac{\partial}{\partial z}\int_{R_r}^{R_o} ru\,\mathrm{dr} - \left[u(R_o)\frac{\partial R_o}{\partial z} - u(R_r)\frac{\partial R_r}{\partial z}\right].$$

Applying the boundary conditions (3) in equation (7), the integrated continuity equation becomes:

$$\frac{\partial}{\partial z}\int_{R_r}^{R_o} ru\,\mathrm{dr}+\frac{\partial}{\partial\theta}\int_{R_r}^{R_o} w\,\mathrm{dr} - w(R_o)\frac{\partial R_o}{\partial\theta} - R_o v(R_o) = 0. \tag{8}$$

The known velocity profiles (eqs. (4) and (5)) are used to evaluate the integrals of w and ru along the radial direction :

$$\begin{aligned}\int_{R_r}^{R_o} w\,\mathrm{dr} \;=\; & \frac{\partial p}{\partial\theta}\frac{R_r}{2\mu}\left\{\frac{1}{2R_r}\left[R_o^2\ln(R_o)-R_r^2\ln(R_r)-(R_o^2-R_r^2)(1+K)\right]+\right.\\ & \left.-R_r\left[\left(\ln(R_r)-\frac{1}{2}+K\right)\ln\left(\frac{R_o}{R_r}\right)\right]\right\}\\ & +\left(\frac{W_{R_o}+R_r^2}{R_o^2-R_r^2}\right)\left[\frac{(R_o^2-R_r^2)}{2}-R_r^2\ln\left(\frac{R_o}{R_r}\right)\right]-R_r^2\Omega\ln\left(\frac{R_o}{R_r}\right),\end{aligned} \tag{9}$$

$$\begin{aligned}\int_{R_r}^{R_o} ru\,\mathrm{dr} = & \left(\frac{\partial p}{\partial z}-\rho g\right)\left(\frac{-R_r^2}{8\mu}\right)\left\{(R_o^2-R_r^2)\left[1-\left(\frac{R_o^2-R_r^2}{2R_r^2}\right)\right.\right.\\ & \left.\left.\left(\frac{1}{R_r^2\ln(R_o/R_r)}\right)\left(R_o^2\ln\left(\frac{R_o}{R_r}\right)-\frac{(R_o^2-R_r^2)}{2}\right)\right]\right\}.\end{aligned} \tag{10}$$

Finally, equation (8) leads to a differential equation that describes the pressure field.

$$\frac{\partial}{\partial\theta}\left(C_1\frac{\partial p}{\partial\theta}\right)+\frac{\partial}{\partial z}\left(C_2\frac{\partial p}{\partial z}\right)=\frac{\partial}{\partial\theta}(C_{0W})+\frac{\partial}{\partial z}(\rho g C_2)+w(R_o)\frac{\partial R_o}{\partial\theta}+R_o v(R_o); \tag{11}$$

where,

$$C_1=\frac{R_r}{2\mu}\left\{\frac{1}{2R_r}\left[R_o^2\ln(R_o)-R_r^2\ln(R_r)-(R_o^2-R_r^2)(1+K)\right]-R_r\left[\left(\ln(R_r)-\tfrac{1}{2}+K\right)\ln\left(\tfrac{R_o}{R_r}\right)\right]\right\},$$

$$C_2=\left(\frac{-R_r^2}{8\mu}\right)\left\{(R_o^2-R_r^2)\left[1-\frac{(R_o^2-R_r^2)}{2R_r^2}+\left(\frac{1}{R_r^2\ln(R_o/R_r)}\right)\left(R_o^2\ln\left(\frac{R_o}{R_r}\right)-\frac{(R_o^2-R_r^2)}{2}\right)\right]\right\},$$

$$C_{0W}=-\left(\frac{W_{Ro}R_o-\Omega R_r^2}{R_o^2-R_r^2}\right)\left[\frac{(R_o^2-R_r^2)}{2}-R_r^2\ln\left(\frac{R_o}{R_r}\right)\right]-R_r^2\Omega\ln\left(\frac{R_o}{R_r}\right).$$

Note that K is the same defined before (eq. (6)) and $\dfrac{\partial R_o}{\partial\theta}$ can be directly derived from the

functions presented in table 1.

Equation (11) is a Poisson equation that describe the pressure field. The boundary conditions are:

- periodic:
  $P(\theta = 0) = P(\theta = 2\pi)$,
  $\frac{\partial P}{\partial \theta}(\theta = 0) = \frac{\partial P}{\partial \theta}(\theta = 2\pi)$.
- imposed pressure at suction and discharge:
  $P(z = 0) = P_{in}$,
  $P(z = L) = P_{out}$.

At each time step, equation (11) was discretized using a central finite difference scheme.

3 NUMERICAL RESULTS

In order to compare and validate the lubrication model, we performed tests at the same liquid and operating parameters used by Sopilka et al. (2002) in their experimental study. The metal singlelobe PCP chosen had the following geometrical characteristics: pump length $L_b = 0.36$ m, length of each rotor pitch $L = 0.06$ m, number of the piches of the rotor $N_r = 6$, radius of the rotor's cross section $R_r = 0.02$ m, radius of the stator's cross section $R_s = 0.020185$ m, eccentricity $E = 0.004039$ m.

In the validation analysis a liquid with a viscosity $\mu = 42$ cP was pumped against a differential of pressure of $\Delta P = 345$ kPa at a rotor angular speed of $\Omega = 300$ rpm.

Figure 6 shows the clearance between the stator and rotor $\delta = R_o(\theta, z) - R_r$ and the predicted pressure field $p(\theta, z)$ at four different times during one cycle of the rotor ($\theta = 0, \pi, 3\pi/2 \text{ and } 2\pi$). The pressure inside the cavity is almost constant and there is a large pressure gradient along the regions of small clearance, the seal lines between the consecutive cavities. The strong pressure gradient is easily observed by plotting. The pressure along the length of the pump at a constant azimuthal coordinate θ, shown in figure 7.

Once the pressure is determined, it is used to evaluate the velocities u and w through the analytical equations (4) and (5). The velocity and pressure at different cross sections ($z_1 = 0.036$m, $z_2 = 0.1764$m, $z_3 = 0.3564$m) of the pump and different times during the rotation ($t_1 = 0.1$s and $t_2 = 0.15$s) of the rotor are shown in figures 8 and 9. Note that the rotor movement squeezes the liquid to flow against the imposed pressure gradient. The plots clearly show the negative axial velocity that represents the back flow caused by the adverse pressure gradient.

The axial velocity profile at the outflow plane of the pump can be integrated in order to evaluate the flow rate through the pump:

$$Q(t) = \int_0^{2\pi} \int_{R_r}^{R_o} \mathbf{u}(L, r, \theta, t) r \mathrm{d}r$$

The predicted flow rate output during one rotation of the pump for two different imposed pressure difference is presented in figure 10. It varies with time as the rotor rotates because of the geometry of cavities. At $\Delta P = 0$, there is no back flow and the flow rate variation is nearly sinusoidal. At $\Delta P = 345$kPa, the back flow reduces the average flow rate, when compared to the previous case, and the flow rate variation with time is far from sinusoidal.

The average flow rate through one cycle of the rotor can be computed as a function of the imposed pressure difference, liquids properties and rotor angular speed in order to construct the pump performance curve, as shown in figure 11. The curves predicted with the model presented here are compared with the experimental data of Sopilka et al. (2002) and with numerical solutions of the complete 3D transient flow obtained using commercial CFD software, presented by Paladino et al. (2008). The comparison was done at $\mu = 42$ and 433 cp, $\Omega = 100$, 300 and 400 rpm. In all cases the agreement was excellent. The relative difference to respect to the experimental data was from 5% to 15%. The larger discrepancies occur at the lower viscosity

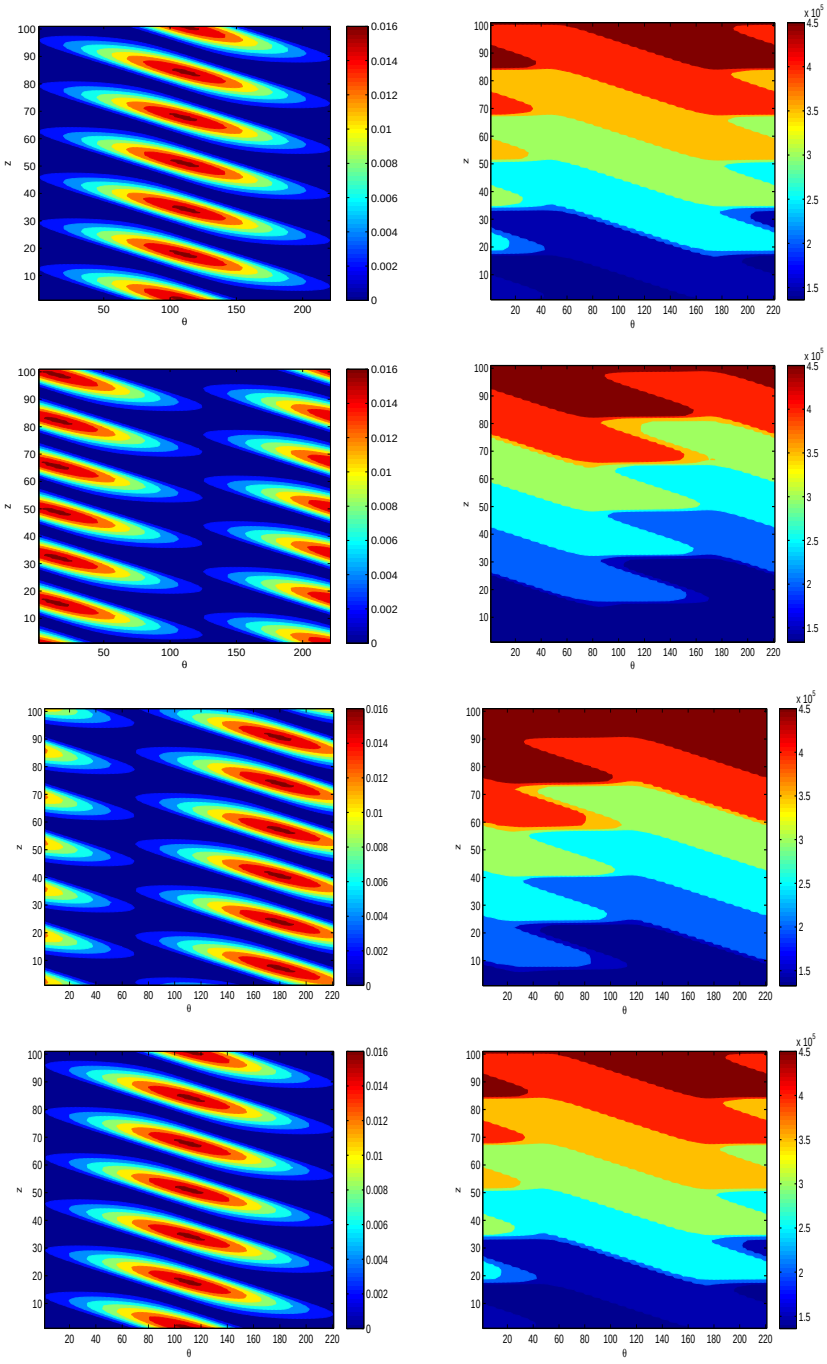

Figure 6: Clearance and pressure distribution in a $\theta \times z$ plane along the time for one turn of the rotor.

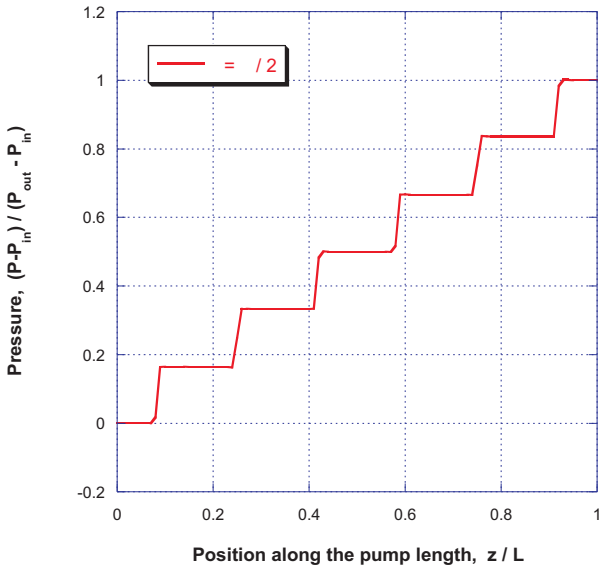

Figure 7: Pressure distribution along pump length

($\mu = 42$ cp) and high pressure difference, conditions at witch the back flow is stronger. With the high viscosity liquid, the back flow is weak and the agreement with the experimental data is nearly perfect.

It is important to emphasize that the computational cost of the predictions obtained with the present model ia orders of magnitude smaller than that required to compute the complete 3D, transient flow presented by Paladino et al. (2008).

It is convenient to define a dimensionless flow rate Q^* as the ratio between the actual flow rate to the volume of the pump times to the rotor frequency. It represents a measure of the pump efficiency:

$$Q^* = \frac{Q_m}{[8\ R_s\ E + \pi\ (R_s^2 - R_r^2)]\ (L/t)}, \tag{12}$$

And the dimensionless pressure difference ΔP^* as:

$$\Delta P^* = \frac{(R_s - R_r)\ \Delta P}{\mu\ \Omega\ R_r} \tag{13}$$

.

All the predictions obtained with the model and presented in figure 11 are plotted in terms of the dimensionless variables in figure 12. The data collapses into one single straight line:

$$Q^* = 0.95 - 8 \times 10^{-5} \Delta P^*$$

With an efficient and accurate model in hand, it can be used as an engineering tool to analyze the effect of different parameters on the pump performance.

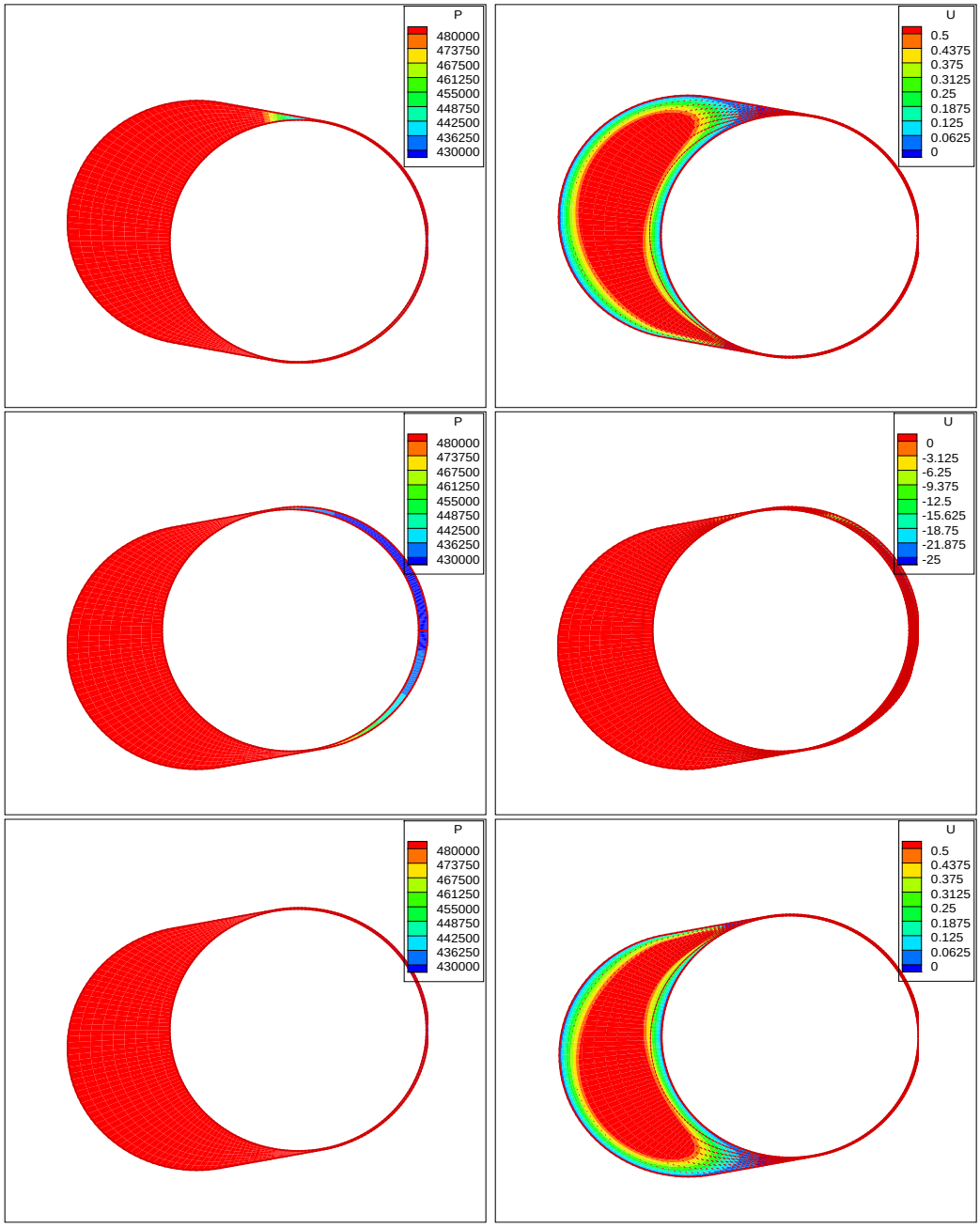

Figure 8: Contour graphs of pressure and velocity fields in the same time ($t_1 = 0.1$s) and three different positions ($z_1 = 0.036$m, $z_2 = 0.1764$m, $z_3 = 0.3564$m.)

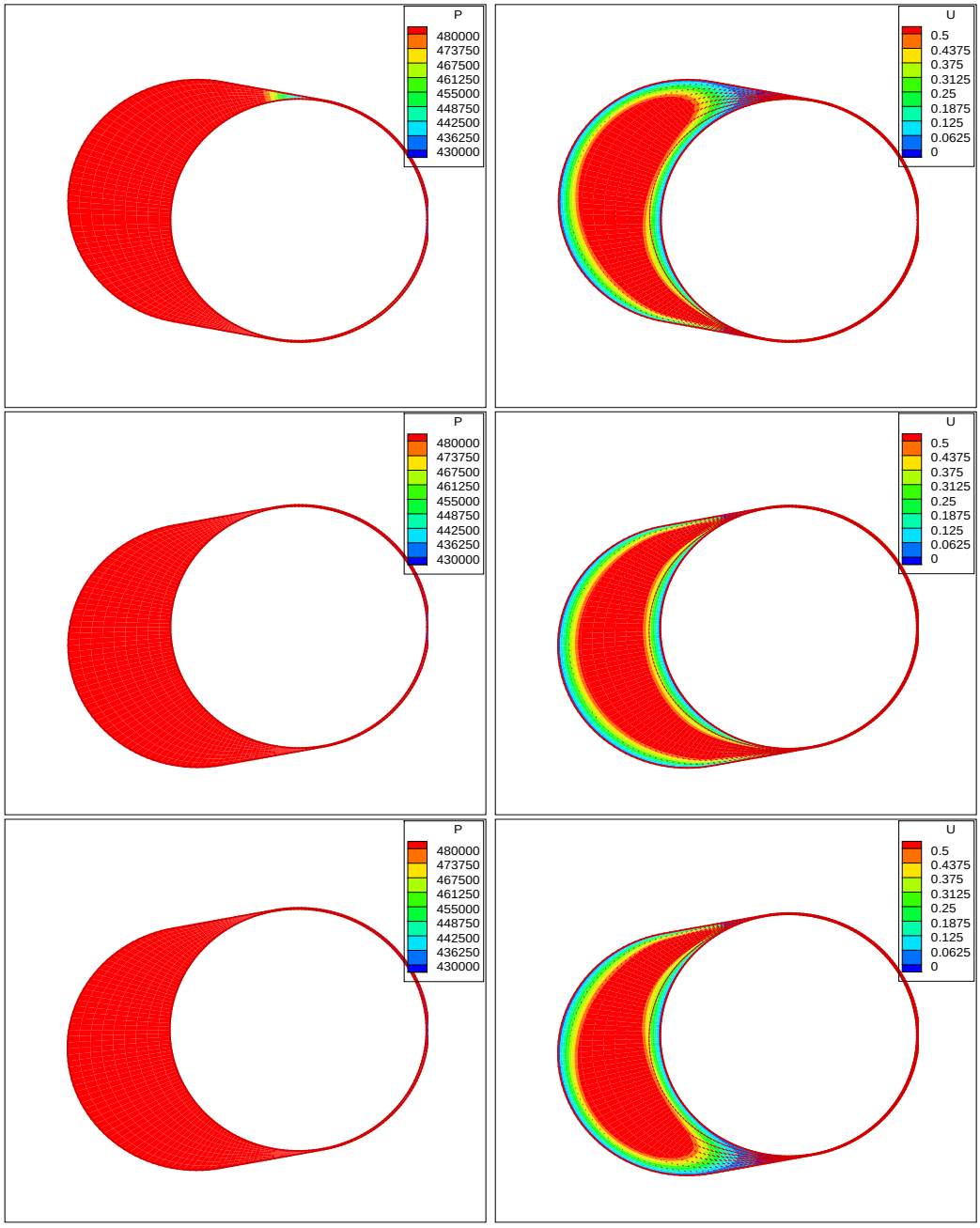

Figure 9: Contour graphs of pressure and velocity fields in the same time ($t_2 = 0.15$s) and three different positions ($z_1 = 0.036$m, $z_2 = 0.1764$m, $z_3 = 0.3564$m.)

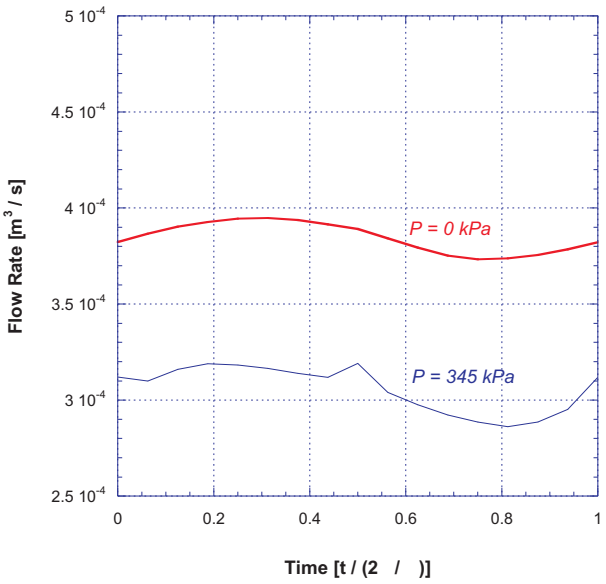

Figure 10: Flow rate versus time. $\Delta P = 0$, $\Delta P = 345$ kPa.

The effect of the clearance $\delta = R_s - R_r$ on the relation between flow rate and imposed pressure difference is showed in figure 13. At larger gaps, the back flow is stronger and the pump efficiency falls drastically. At hight enough pressure difference, the flow rate is negative, indicating that the pump can not move liquid against that hight pressure difference. At small clearance, the flow rate dependence on pressure difference is weaker and the pump efficiency is higher.

4 CONCLUSIONS

In this work, an asymptotic model for the flow inside a metallic (rigid) singlelobe progressive cavity pump was developed. The cross section is parameterized using cylindrical coordinates and there is no simplified assumption of the geometry and kinematics of the rotor. The proposed model reduces the three-dimensional transient Navier-Stokes equation to a quasi-steady state two-dimensional Poisson's equation for the pressure field and provide detailed information about the flow inside the pump. The resulting 2D equation for the pressure field at each time step was discretized with a second order finite difference approximation. The model was used to obtain predictions of the pump performance curve as a function of rotor speed, liquid properties and pump geometry. The results obtained agree very well with experimental data and with the complete 3D model and the computational time required was orders of magnitude smaller when compared to the later. Because of the accurate and efficient computation, the model can be integrated into a flow simulator with PCPs and also be used on design of new pumps. Another interesting characteristic of this asymptotic model is that it can be extended to PCPs with deformable stator, different geometries and also multiphase flows.

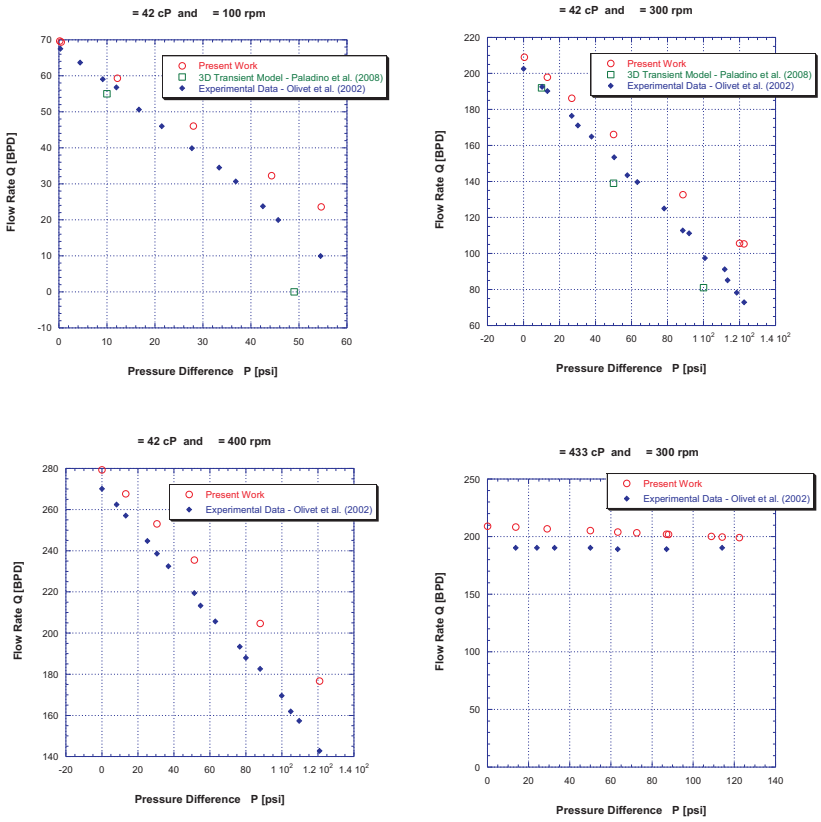

Figure 11: μ = 42cP and 433cP, rotor velocity 100, 300 and 400rpm

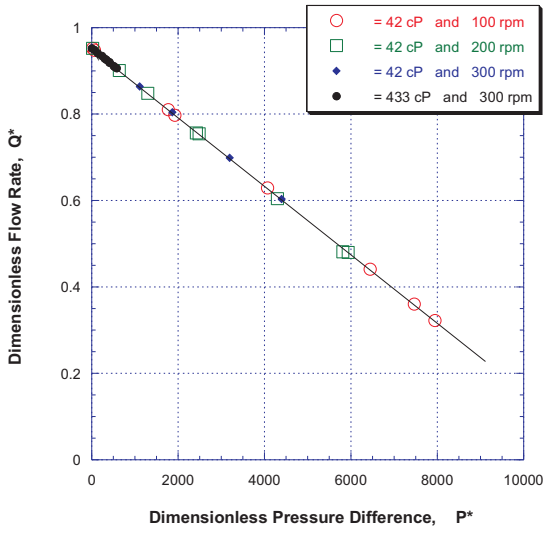

Figure 12: $Q^* \times \Delta P^*$

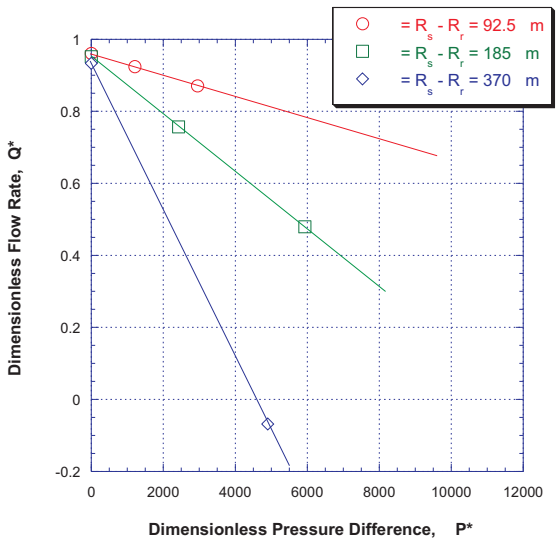

Figure 13: The clearance effect.

REFERENCES

Blanco J.A.G. and Olivet A. New approach for modelling progressive cavity pumps performance. *Society of Petroleum Engineers - SPE*, 84137, 2003.

Carvalho M.S. and de Pina E.P.F. Three-dimensional flow of a newtonian liquid through an annular space with axially varying eccentricity. *Jounal of Fluids Engineering*, 128:226–230, 2006.

Cholet H. *Progressive Cavity Pumps*. Editions Technip, Paris, 1997.

Li Y. H.F. Modeling of flow in a single screw struder. *Journal of Food Engineering*, 27(4):353–375, 1996.

Moineau. A new capsulism. *Doctoral Thesis*, 1930.

Paladino E.E., Lima J.A., and Almeida R.F. Computing modeling of the three-dimensional flow in a metallic stator progressing cavity pump. *Society of Petroleum Engineers - SPE*, 114110, 2008.

Sopilka A.J.O., Blanco J.A.G., and Kenvery F. Experimental study of two-phase pumping in a progressing cavity pump metal to metal. *Society of Petroleum Engineers SPE*, 77730, 2002.

Suresh A. Chakraborty S. K.K.G.S. Low-dimensional models for describing mixing effects in reactive extrusion of polypropylene. *Chemical Engineering Science*, 63(14):3788–3801, 2008.